Published in final edited form as:
Biochemistry. 2011 March 29; 50(12): 2264–2273. doi:10.1021/bi1013694.

Atomic View of Calcium-Induced Clustering of Phosphatidylserine in Mixed Lipid Bilayers†

John M. Boettcher[‡,#], **Rebecca L. Davis-Harrison**[§,#], **Mary C. Clay**[‡], **Andrew J. Nieuwkoop**[‡], **Y. Zenmei Ohkubo**[§,||,¶], **Emad Tajkhorshid**[§,||,¶,⊥], **James H. Morrissey**[§,⊥], and **Chad M. Rienstra**[*,‡,§,||]

[‡] Department of Chemistry, University of Illinois at Urbana-Champaign, Urbana, Illinois 61801

[§] Department of Biochemistry, University of Illinois at Urbana-Champaign, Urbana, Illinois 61801

[||] Center for Biophysics and Computational Biology, University of Illinois at Urbana-Champaign, Urbana, Illinois 61801

[¶] Beckman Institute, University of Illinois at Urbana-Champaign, Urbana, Illinois 61801

[⊥] College of Medicine, University of Illinois at Urbana-Champaign, Urbana, Illinois 61801

Abstract

Membranes play key regulatory roles in biological processes, with bilayer composition exerting marked effects on binding affinities and catalytic activities of a number of membrane-associated proteins. In particular, proteins involved in diverse processes such as vesicle fusion, intracellular signaling cascades, and blood coagulation interact specifically with anionic lipids such as phosphatidylserine (PS) in the presence of Ca^{2+} ions. While Ca^{2+} is suspected to induce PS clustering in mixed phospholipid bilayers, the detailed structural effects of this ion on anionic lipids are not established. In this study, combining magic angle spinning (MAS) solid-state NMR (SSNMR) measurements of isotopically labeled serine headgroups in mixed lipid bilayers with molecular dynamics (MD) simulations of PS lipid bilayers in the presence of different counterions, we provide site-resolved insights into the effects of Ca^{2+} on the structure and dynamics of lipid bilayers. Ca^{2+}-induced conformational changes of PS in mixed bilayers are observed in both liposomes and Nanodiscs, a nanoscale membrane-mimetic of bilayer patches. Site-resolved multidimensional correlation SSNMR spectra of bilayers containing ^{13}C, ^{15}N-labeled PS demonstrate that Ca^{2+} ions promote two major PS headgroup conformations, which are well resolved in two-dimensional ^{13}C-^{13}C, ^{15}N-^{13}C and ^{31}P-^{13}C spectra. The results of MD simulations performed on PS lipid bilayers in the presence or absence of Ca^{2+} provide an atomic view of the conformational effects underlying the observed spectra.

In healthy cells, phosphatidylserine (PS) resides on the inner leaflet of the plasma membrane (1) and represents 10–20% of all plasma membrane lipids (2,3). PS both imparts a negative surface potential for nonspecific binding of cationic proteins (4,5) and recruits several proteins through specific interactions, frequently involving Ca^{2+} (6). Externalization of PS in activated platelets and apoptotic cells constitutes a signal eliciting coagulation and

†This work was supported by the National Institute of General Medical Sciences, NIH (R01-GM075937 and R01-GM079530 to C.M.R., and R01-GM086749 and R01-GM067887 to E.T.), the National Center for Research Resources, NIH (P41-RR05969 to E.T.), the National Heart Lung and Blood Institute, NIH (R01 HL47014 to J.H.M. and R01 HL103999 to J.H.M. and C.M.R.), and by the American Heart Association (0920045G to R.D.H.).

[*]To whom correspondence should be addressed: Chad Rienstra, Dept. of Chemistry, University of Illinois at Urbana-Champaign, 600 S Mathews Ave, Box 50-6, Urbana, IL 61801, Phone: 217-244-4655. Fax: 217-244-3186. rienstra@scs.uiuc.edu.
[#]These two authors contributed equally to this work.

phagocytosis, respectively (7,8). It is well documented that relatively high concentrations of Ca^{2+} can exert dramatic effects on membranes containing PS, observed as alterations in phase transition and separation of lipid components leading to aggregation, fusion, and even collapse of the membrane bilayer structure (9–12). However, Ca^{2+} in the cytoplasm is tightly controlled at much lower levels, around 100 nM for a quiescent cell, increasing 10 to 100-fold (to ~μM) for an activated cell (13), while plasma contains about 2.4 mM total Ca^{2+}. At physiologically relevant concentrations, Ca^{2+} may exert more subtle effects on a bilayer structure that are challenging to measure but of potential importance to the timing and coordination of many cellular processes.

Microscopic and transient islands enriched in specific lipids are proposed to act as targets enhancing and/or coordinating activities such as cell signaling and blood coagulation (14,15). To date, most investigations of divalent cation- and protein-induced PS microdomains have either relied on perturbative methods or focused on bulk characteristics such as surface pressure (15–17). For instance, it has been demonstrated that membrane-binding proteins, such as annexin A5 and 2, in concert with plasma concentrations of Ca^{2+} induce the lateral organization of anionic phospholipids such as PS, phosphatidic acid (PA) and phosphatidylinositol (4,5)-bisphosphate (PIP_2) (16,18,19). Recently, fluorescence microscopy has revealed that plasma Ca^{2+} concentrations induce clustering of PIP_2 into sub-micrometer domains, but no such effect was observed for PS (20). Intriguingly, fluorescence microscopy previously revealed micrometer scale clustering for PA (19), and more detailed infrared vibrational spectroscopic studies using plasma levels of Mg^{2+} showed clustering of DPPS into groups of 10–100 acyl chains (17), well below the resolution of light microscopy (17). This suggests that Ca^{2+}-induced lateral organization of PS may occur at a limited scale on the order of $\sim 10^2$ lipids. A few previous NMR studies have shown that Ca^{2+}-PS interactions in mixed bilayers cause conformational changes in PS headgroups (21,22), but only structures of PS headgroups in the absence of Ca^{2+} are currently available (23). Thus, a detailed molecular model of exactly how Ca^{2+} ions interact with PS molecules at a membrane surface has yet to emerge and may provide clues important for unraveling why the lateral organization of PS seems to occur at different size scales from other anionic phospholipids.

Piecing together what is known about a few Ca^{2+}-dependent membrane-binding domains, and what is predicted about the PS lipid bilayer structure, suggests that the bulk of PS-bound Ca^{2+} resides in the phosphodiester region of the bilayer, and that the PS headgroup rigidifies upon Ca^{2+} binding. For instance, several Ca^{2+}-dependent C2 domains penetrate the bilayer sufficiently to position their Ca^{2+} binding sites within the phosphodiester linker region of the membrane (24–26), and a similar behavior has been predicted in a recent model for GLA domains (27). It has also been reported that PS increases the apparent binding affinity of Ca^{2+} to the zwitterionic lipid, phosphatidylcholine (PC), if an excess of Ca^{2+} in the electrical double layer due to the formal negative charge of PS is taken into account (i.e., the amount of Ca^{2+} bound by either PS or PC is correlated with the concentration of Ca^{2+} directly adjacent to the bilayer) (28). Both observations hint that Ca^{2+} is most likely intercalated within the phosphodiester layer of the membrane, and in such a position it would rigidify not only PS headgroups but also perhaps the glycerol backbone of PS and neighboring PC headgroups. Indeed, molecular dynamics (MD) investigations concur with this hypothesis, demonstrating that Ca^{2+} predominantly resides within ~10 Å of the phosphodiester moiety, and may be found associated to a lesser extent with the PS carboxyl (29,30). Whether Ca^{2+} preferentially binds the PS phosphate or carboxyl has not been observed directly, and may have biological consequences in promoting or limiting the lateral organization of PS.

In this study, we investigate the interactions of Ca^{2+} with PS-containing lipid bilayers using all-atom MD simulations paired with magic angle spinning (MAS) solid-state NMR

(SSNMR) studies that employ two membrane mimetics, liposomes and Nanodiscs. Nanodiscs are discoidal phospholipid bilayers of 8 nm-diameter containing ~67 lipids per leaflet which are wrapped and stabilized by two molecules of an amphipathic helical protein termed membrane scaffold protein (MSP) (31–34). Many studies have effectively used the Nanodisc system as a membrane mimetic to study membrane protein interactions (35,36), including SSNMR analyses of membrane protein structures (37–39). One advantage of the Nanodisc system, in addition to precise local control over lipid composition, is that their structural integrity is maintained in the presence of mM concentrations of Ca^{2+}, even with up to 90% PS in the bilayer—as opposed to liposomes which cannot tolerate more than ~30% PS in the presence of Ca^{2+} without undergoing vesicle aggregation, fusion and collapse. For these reasons, the Nanodisc system is an ideal experimental platform for investigating nanoscale Ca^{2+}-PS interactions on a membrane surface by SSNMR.

In the present study, the serine headgroup of PS has been isotopically labeled and incorporated into the lipid bilayers, allowing high-resolution NMR spectra of PS headgroup moieties interacting with Ca^{2+} ions. Our results indicate that Ca^{2+} ions promote the formation of a more ordered liquid phase, producing rigid conformations for PS headgroups. Mobility of the lipid acyl chains is not as affected by interactions with Ca^{2+} ions as the headgroups, although alteration of the phase transition behavior of the bilayer by Ca^{2+}-PS interactions is presented. We report carbon, nitrogen and phosphorus chemical shift values for two Ca^{2+}-induced PS conformations as well as initial estimates of intermolecular distances between the two PS conformations in the bilayer. Furthermore, all-atom MD simulations performed in conjunction with NMR measurements support the idea of the Ca^{2+}-induced lateral reorganization of PS and indicate a much tighter fluctuation radius for Ca^{2+} over Na^{+} at the PS phosphodiester and carboxyl moieties. In the simulations, two predominant conformational species are also observed. These two PS conformations may be a basis for Ca^{2+}-induced lateral organization of PS molecules.

EXPERIMENTAL PROCEDURES

Isotopically Labeled POPS

In a modification of the method of Iwasaki *et al.* (40), phospholipase D from *Streptomyces* (PLD; Sigma-Aldrich, St. Louis, MO) was used to replace the choline headgroup of POPC (1-palmitoyl-2-oleoyl-phosphatidylcholine) with U-^{13}C, ^{15}N-L-serine (Cambridge Isotopes Laboratories, Andover, MA) to yield POPS (1-palmitoyl-2-oleoyl-phosphatidylserine) isotopically labeled in the serine headgroup (termed POPS*). Briefly, 5 μg/mL PLD was added, with stirring, to a mixture of 1.5 M ^{13}C, ^{15}N-serine, 36 mg/mL POPC (Avanti Polar Lipids, Alabaster, AL) and $CaSO_4$ in 50 mM sodium acetate buffer, pH 5.6, and allowed to react overnight at 42 °C. The supernatant was collected by centrifugation, flushed with nitrogen gas and stored at 4 °C for use in subsequent reactions. The pellet was washed with water and re-suspended in 2:1 hexane:ethanol (5 mL per 1 mL original reaction volume), followed by water (1/4 the volume of hexane:ethanol) and 1 N HCl (1/10 the volume of the water). After vortexing, the hexane phase was collected, and the aqueous phase and pellet were extracted with additional hexane. The pooled hexane phases were dried under vacuum and POPS* was purified by CM52 chromatography (41). Purity of POPS* was evaluated by two-dimensional thin-layer chromatography, using 90:54 chloroform:methanol for the first dimension and 65:25:4 chloroform:methanol:water for the second dimension. When necessary, POPS* was further purified by flash silica chromatography developed with 90:40:12:2 chloroform:methanol:acetic acid:water. Purified POPS* was stored in chloroform and its concentration determined by inorganic phosphate analysis after complete hydrolysis. POPS* purity and the level of ^{13}C, ^{15}N-serine incorporation was verified by HSQC solution NMR in chloroform.

Nanodisc Preparation

Nanodiscs were prepared as previously described (33) using mixtures of POPC and POPS*. After the Nanodiscs were assembled, they were purified by size-exclusion chromatography (33), except that the buffer was 10 mM Tris-HCl pH 7.4, 10 mM NaCl, with 2 mM $CaCl_2$. Samples were concentrated using an Amicon Ultra 10000 NMWL centrifugal filter (Thermo Fisher Scientific, Waltham, MA) to 2–3 mM phospholipid (15–22 μM Nanodiscs). The lyoprotectant, trehalose, was added in a 1:1 molar ratio to phospholipid, after which samples were frozen and lyophilized. The powders (~50% Nanodiscs by weight) were packed into 3.2 mm SSNMR rotors, after which water was added (equal to ~50% of the dry weight of packed samples).

Liposome Preparation

Mixtures of dried POPC and POPS* (10 mg total) were suspended in 30 μL of 50 mM Tris-HCl pH 7.4, 100 mM NaCl, 2.5 mM $CaCl_2$ and sonicated until the solution was visually homogeneous, after which 1 mL of 2.5 mM $CaCl_2$ was added and the solution was sonicated again. Sample preparation in the absence of Ca^{2+} was identical except for the inclusion or addition of $CaCl_2$. Liposomes were collected by ultracentrifugation at 4 °C for 2.5 hours at 250,000 rcf, and the pelleted liposomes were packed into 3.2 mm SSNMR rotors.

SSNMR

SSNMR studies were performed on four-channel Varian InfinityPlus spectrometers. POPS*:POPC Nanodisc spectra were acquired at 600 MHz with a Varian T3 ^{1}H-^{13}C-^{15}N 3.2 mm probe at an MAS rate of 10,000±3 Hz. The variable temperature gas was maintained at 90±10 scfh flow, and the reported sample temperatures take into account thermocouple calibration and frictional heating due to MAS, as calibrated with ethylene glycol (42). All experiments utilized tangent ramped cross polarization (CP) (43) with TPPM (44) decoupling of the protons applied during acquisition and evolution periods on average at ~80 kHz. Data were processed with NMRPipe (45) with back linear prediction and polynomial baseline (frequency domain) correction applied to the direct dimension, and zero filling and Lorentzian-to-Gaussian apodization applied to each dimension before Fourier transformation; additional processing parameters are located in the figure captions. Chemical shifts are referenced to adamantane, using the IUPAC standard gyromagnetic ratios to indirectly reference ^{15}N and ^{31}P spectra (46). Peak picking and assignments were performed with Sparky (47).

MD Simulations

Two systems, each consisting of 288 1,2-dioleoyl-*sn*-glycero-3-[phospho-L-serine] (DOPS), were simulated in the presence of two different counterions. The first system included 144 Ca^{2+} ions and the other 288 Na^{+} ions. Each system was simulated for 100 ns under NP_nTA conditions using NAMD 2.6 (48) with the CHARMM27 set of force field parameters (49). Periodic boundary conditions were assumed and the particle mesh Ewald (PME) method (50) was employed for the computation of long-range electrostatic interactions without truncation. A constant area of 9,409 $Å^2$ (97 Å × 97 Å) was imposed for both systems to maintain an experimentally obtained area-per-lipid value (51). The details of the simulations are identical to those described elsewhere (27,52). The last 90 ns of the trajectories were used for analysis.

RESULTS

Effects of Ca^{2+} Binding on ^{13}C Chemical Shifts in PS Headgroups

To test the effect of Ca^{2+} on PS headgroup conformation, we initially compared one-dimensional ^{13}C spectra of mixed POPS*:POPC bilayers, observing the effects of Ca^{2+} on the ^{13}C chemical shifts, which are sensitive to binding events and structural changes. (POPS* is phosphatidylserine whose L-serine headgroups are uniformly labeled with ^{13}C and ^{15}N.) One-dimensional CP ^{13}C spectra (Figure 1) were acquired on liposomes containing 30% POPS*, 70% POPC in the absence (Figure 1a, b) and presence (Figure 1c, d) of 2.5 mM Ca^{2+}. We observe narrow resonances due to natural abundance ^{13}C on the fatty acyl chains (predominantly at 25 to 40 ppm, but also the ~132 ppm resonance ascribed to the olefinic carbons in the oleoyl chain), which are consistent with previous SSNMR assignments of lipids in bilayers (53). Above the phase transition (10 °C, Figure 1b) in the absence of Ca^{2+}, the POPS* headgroup signals are narrow and strong, when observed via direct (^{13}C Boltzmann) polarization in Bloch decay experiments (data not shown), yet cross polarize weakly from protons, indicative of fast-limit motions averaging dipolar couplings to a nearly isotropic limit. When frozen in the absence of Ca^{2+} (−20 °C, Figure 1a), the gel phase spectrum exhibits broad features characteristic of the inhomogeneous distribution of headgroup environments, since no particular conformation is preferred. In contrast, spectra of liposomes at −20 °C in the presence of 2.5 mM Ca^{2+} (Figure 1c) contain distinct ^{13}C resonances from POPS* headgroups, which cross polarize with high efficiency and have the typical characteristics of a rigid solid (e.g., cross polarization buildup in hundreds of microseconds and a requirement for high power decoupling to observe well-resolved spectra). Two resonances, at 66.3 and 67.9 ppm, are tentatively assigned to the POPS* alpha carbon (Cα), while upfield POPS* peak at ~60 ppm is significantly broadened (line width 190 Hz), potentially arising from two unresolved beta carbon (Cβ) signals (we remind readers that the lipid nomenclature for PS headgroups differs from that used for amino acids; i.e., the carbon proximate to the ^{31}P is called Cα). Similarly, the POPS* gamma carbon (Cγ) (at ~174.2 ppm) resonance is also slightly broadened to 131 Hz, which, while not as dramatic as the Cβ, is still consistent with two unresolved signals.

We propose that the carbon chemical shifts of the PS headgroup are the result of two distinct chemical environments in the presence of Ca^{2+} that are long-lived on NMR time scales (>10 ms). This hypothesis is compatible with earlier studies (21,22) showing that PS headgroups, in mixed bilayers, adopt a rigid conformation in the presence of Ca^{2+}. To test whether this rigidity is sufficient to maintain near rigid-lattice behavior of the lipid headgroup above the phase transition, we also performed experiments with Ca^{2+}-treated liposomes at 10°C (Figure 1d). Under this condition, the POPS*:POPC liposomes exhibited the same splitting of the POPS* Cα, and broadening of the POPS* Cβ and Cγ resonances, as in spectra acquired at −20 °C (Figure 1c). Again, these results agree with the results reported by Roux *et al*., where the conformational changes were observed with Ca^{2+} and membrane mimetics in solution NMR experiments at 25 °C, well above the phase transition (22).

We also investigated the effect of Ca^{2+} on PS headgroups using POPS*:POPC Nanodiscs in the presence of 2 mM Ca^{2+}, containing either 30% POPS* (Figure 1e, f) or 70% POPS* (Figure 1g, h), both above (+10 °C, Figure 1f, h) and below (−20 °C Figure 1e, g) the phase transition. One-dimensional ^{13}C spectra are consistent with the spectra of similarly treated liposomes shown in Figure 1a–d, with identical chemical shifts observed for the POPS* headgroup carbons. These data show that the same Ca^{2+}-induced PS conformations are present in both liposomes and nanoscale bilayers over a broad range of PS concentrations.

Ca^{2+}-PS Interactions Alter the Phase Transition and Dynamics of Lipids within the Bilayer

A first experimental investigation of Ca^{2+}-induced PS microdomain dynamics was performed by examining the change in the apparent phase transition of the mixed POPS:POPC Nanodisc bilayers in the presence of Ca^{2+}. ^1H transverse relaxation (T_2) values of directly detected ^1H spectra over a ±20 °C temperature range reveal acyl chain dynamics as a function of temperature (Figure 2a). We confirmed the expected ~3 °C phase transition of pure POPC Nanodisc bilayers observed in previous differential scanning calorimetry measurements (54). Dynamics measurements on mixed lipid POPS*:POPC Nanodiscs with 2 mM Ca^{2+} (Figure 2a) display a broadened (spanning about a 30 °C range) and slightly elevated phase transition in comparison to POPC Nanodisc. This effect has been reported previously using other membrane mimetics (28, 55, 56) and is attributed to the Ca^{2+}-PS coordination.

A control study was performed on the POPC Nanodisc bilayer to investigate the lateral diffusion and mobility of lipids inside the Nanodiscs and to identify any possible interactions between the lipid acyl chains and the MSP protein that might distort the phase transition (i.e., to identify whether a perturbed boundary layer of lipids exists in Nanodiscs). The ^1H T_2 (at 25°C) of the methylene protons neighboring the olefinic bond (carbon positions 8 and 11 in Figure 1), unique to the lipid acyl chain, were measured to prevent spurious contributions from MSP protons (Figure 2b). A single exponential fit best described the decay behavior (Figure 2b), indicating that all the lipids are fully mobile within the Nanodisc and diffuse freely on NMR time scales. Thus, any interactions between lipids and the membrane scaffold protein occur in the rapid exchange regime and therefore have only negligible effects on the phase transition.

To further understand the dynamics of Ca^{2+} on the POPS*:POPC bilayers, a more detailed, site-specific investigation of the bilayer dynamics was performed. Site-specific dynamics measurements using SSNMR recoupling methods were performed for POPS*:POPC Nanodisc bilayers utilizing the symmetry-based sequence $R18_1^7$ (57), which reports on ^1H-^{13}C dipolar couplings. The $R18_1^7$ sequence recouples the ^1H-^{13}C-dipolar interactions, and signal intensity measured as a function of time reports on the dynamics of the system. Observed here are the ^1H-Cα (Figure 3a) and ^1H-Cβ (Figure 3b) dephasing curves due to ^1H-^{13}C-dipolar interactions of the POPS* headgroup at varying temperatures. The bulk acyl chain trajectory (Figure 3c) shows that at −30 °C, the ^{13}C signal dephases to 30% of its original intensity within 180 microseconds and at −5 °C this happens within 190 microseconds, but at +5 °C the dephasing requires 220 microseconds and at +20 °C, 240 microseconds. In contrast, the headgroup ^{13}C signal (Figure 3a, b) dephases to 30% of its original intensity within 100 microseconds, which is in the rigid lattice regime where the order parameter is ~0.9 or higher (depending on normalization of the ^1H-^{13}C bond length), independent of temperature. The order parameter for the acyl chain is approximately 0.5 at +20 °C. Thus, the serine headgroups have very little change in order parameter over a temperature range of −30 to +20 °C in the presence of Ca^{2+} ions (Figure 3). In contrast, the acyl chains' motions are activated over the same temperature range, becoming approximately twice as mobile as the temperature is increased. This result is consistent with the model in which the POPS lipids form microdomains when the headgroups are restrained in position by the presence of Ca^{2+} ions (likely also restraining lateral diffusion), while the acyl chains have fewer restrictions to motional modes such as axial diffusion and trans-gauche isomerization.

Ca^{2+}-PS Interactions Observed in All-Atom Simulations

To gain further insight into the ordering of the PS-containing membranes, we have investigated the effect of the counterion on PS headgroups by all-atom MD simulations.

Pure DOPS membrane patches were prepared with either Ca^{2+} or Na^{+} as counterion and simulated each for 100 ns. Structural comparison of the two systems clearly indicates Ca^{2+}-induced organization of the PS headgroups, as demonstrated by the decrease in fluctuation of the phosphate and carboxyl groups of the lipids illustrated in Figure 4. Distinct patterns of Ca^{2+} and PS headgroups are evident (Figure 4, top right panel) indicating lateral organization of PS headgroups within the membrane environment in the presence of Ca^{2+} ions, an effect that is smaller in the Na^{+} system and in line with the fact that residence times for cation-lipid interactions are shorter for Na^{+} compared to Ca^{2+}. Even though the time scale of the simulations is shorter than the time scales that fully capture the conformational dynamics measured in the NMR measurements, structural analysis of the results can shed light on the putative conformations that might represent the two PS populations detected in the NMR measurements (which we term PS1 and PS2). In the simulations, two major conformational populations are observed for the lipid headgroups, with regard to the O-Cα-Cβ-N dihedral angle. These populations are the two gauche conformations of the serine headgroup, with average dihedral angles of around −60 and 60 degrees respectively; these dihedral angels correspond to P-Cγ distances centered around ~4.5 Å and ~5.1 Å, which are the distances derived for PS1 and PS2 from the NMR measurements. A snapshot showing a PS1 and a PS2 joined by a common Ca^{2+} ion is shown as an inset in Figure 7. The Ca^{2+} counterions themselves are also significantly immobilized (average RMSF, 3.45 ± 1.10 Å) by interacting with the phosphate and carboxyl groups, whereas Na^{+} moves rather rapidly from one headgroup to another on the order of a few nanoseconds, thus traveling a long range on the membrane patch within the time scale of the simulation (average RMSF, 12.41 ± 3.51 Å).

Two-Dimensional Spectra of POPS*:POPC Nanodiscs

Using a series of two-dimensional spectra (Figure 5) acquired on 70% POPS*, 30% POPC Nanodiscs in the presence of 2 mM Ca^{2+}, we site-specifically assigned the chemical shifts of the two PS headgroup conformations and report on their intra- and intermolecular correlations. We acquired ^{13}C-^{13}C, ^{15}N-^{13}C, and ^{31}P-^{13}C two-dimensional spectra (Figure 5) and assigned the chemical shifts for both PS spin systems (Table 1) for all carbon, nitrogen and phosphorus atoms. We arbitrarily refer to the two spin systems PS1 and PS2 (Table 1). The ^{13}C-^{13}C two-dimensional spectra were acquired with 25 and 200 ms of DARR mixing (58,59) (Figure 5a, b). The carbon signals arising from the naturally abundant ^{13}C on the acyl chains are observed along the diagonal below 40 ppm; as expected, no cross peaks observed in this region. ^{13}C-^{13}C spectra with 25 ms DARR mixing (Figure 5a) show intramolecular Cα-Cβ cross peaks of both PS1 and PS2. The ratio of integrated intensities of the PS1:PS2 intramolecular Cα-Cβ cross peaks is 50:50, indicating that the PS is divided approximately equally between the two conformations. Additionally, intramolecular Cα-Cγ and Cβ-Cγ correlations are observed for both conformations. Similar intramolecular correlations are observed between both ^{15}N and ^{31}P of the two PS conformations and the three carbon resonances (Cα, Cβ, Cγ) in the ^{15}N-^{13}C and ^{31}P-^{13}C two-dimensional TEDOR (60) spectra (Figure 5c, d).

Intra- and intermolecular correlations in the two-dimensional spectra reveal structural insights of individual PS headgroups and on the lateral organization of the two conformations, respectively. TEDOR (heteronuclear) (60), DARR (homonuclear, ^{13}C-^{13}C) (58,59), and ^{1}H diffusion (CHHC) (homonuclear, ^{1}H-^{1}H) (61,62) pulse sequences take advantage of strong dipolar interactions present in SSNMR. The dipolar interaction is a through-space interaction and therefore inherently contains information on distance ($\propto 1/r^3$) that is reflected in the intensity of the cross peaks as a function of mixing time. Using the ^{1}H-^{1}H, ^{13}C-^{13}C, and ^{13}C-^{31}P dipolar interactions, distances up to ~6 Å can be measured

between atoms. The ^{31}P-^{13}C TEDOR spectrum (Figure 5d) exhibits P-Cγ and P-Cβ intramolecular cross peaks with differing intensities for the PS1 and PS2 conformations.

Finally, using ^{13}C-^{13}C DARR spectrum with 200 ms mixing (Figure 5b), and CHHC spectra with 100 and 400 μs mixing (Figure 6) we show direct evidence of Ca^{2+}-induced PS lateral organization. Both types of 2D ^{13}C-^{13}C spectra show cross peaks between the Cα of PS1 and the Cα of PS2. These experiments both support the semi-quantitative restraint on the intermolecular ^{13}C-^{13}C distance of less than 6 Å, based on previous studies that have calibrated these methods (61, 62). The fact that such correlations are observed in the CHHC experiment at less than 1 ms mixing time furthermore illustrates that chemical exchange could not account for the observed cross peaks, since rates of exchange on this timescale would lead to substantial line broadening in the NMR spectra. To provide a compelling quantitative measurement of the intermolecular arrangements, we collected a trajectory of mixing times from the 3D ZF-TEDOR experiment (63), utilizing ^{31}P and ^{15}N, for which the complication of homonuclear scalar and dipolar couplings is minimized. The intermolecular ^{31}P-^{15}N distance fits to 6.1 Å (Figure 7). Altogether, the multiple observations of intermolecular cross peaks and dipolar coupling confirm a tight packing of the PS headgroups in the presence of Ca^{2+} ions, and give insight into the geometric arrangement of the PS conformations.

DISCUSSION

Ca^{2+} is thought to induce the formation of PS microdomains in mixed lipid bilayers and has previously been shown to induce rigid PS headgroup conformations (21,22). The interaction of PS with Ca^{2+} has also been shown to affect the bulk properties of the bilayer and indicate the formation of larger PS microdomains. However, observations of the phenomena have not resolved the scale of the PS assemblies formed with Ca^{2+} (in particular), nor have key features of the molecular structure of such assemblies been reported. Our observations using POPS*-enriched liposomes and Nanodiscs now demonstrate the formation of two distinct, rigid PS headgroup conformations induced upon interaction with Ca^{2+}, that are within ~6 Å of each other. We also report the site-specific assignments of headgroup nitrogen, carbon and phosphorus resonances for the two PS headgroup conformations, PS1 and PS2 (Table 1) and give preliminary distance measurements that report on their structure. Previously, Sanson *et al.* reported two headgroup conformers solved at pH 7.5 for the PS headgroup of 1,2-dimyristoyl-phosphatidylserine (DMPS) in dodecylphosphocholine (DPC) micelles (23). That report (23) focused on the conformation of the glycerol backbone of the lipids and no angular or distance data were specifically reported for the serine headgroups. This makes comparing our preliminary distance data with previous structures difficult, so we cannot exclude or confirm the existence of those structures in the Ca^{2+}-induced PS domains. Significantly, we observe a major change (reduction) in the dynamics of the conformations in the presence of Ca^{2+}. PS conformers in the presence of Na^{+} are in fast chemical exchange, sampling many conformations over the NMR chemical shift timescale (23,64). Therefore, this fast exchange among conformations in the absence of Ca^{2+} results in only one chemical shift value for each of the three carbons (Cα, Cβ, Cγ) above the phase transition temperature and broad signals below it (Figure 1). Addition of Ca^{2+} to the system coordinates PS into two distinct conformations, changing the dynamics of the system, so that PS1 and PS2 are long-lived on the NMR timescale.

In addition to the change in headgroup dynamics, the results show a marked change in the bulk dynamics of the bilayer. The dynamics measurements using the Nanodisc system demonstrate that Ca^{2+} interactions observed with mixed POPS:POPC bilayers are consistent with previous studies using liposomes (21,22,28,65). Site-specific dynamics data (Figure 3) indicate that interactions of Ca^{2+} with mixed POPS:POPC bilayers cause the PS headgroups

to become highly ordered, while the acyl chains are only slightly affected by this ordering. This observation has been made previously and indicates that in the presence of Ca^{2+}, the PS headgroups do not dominate the properties of the hydrophobic tails in the liquid-crystalline state (65). This explains the increase in the liquid-crystalline to solid-gel phase transition temperature of these mixed bilayers presented here (Figure 2a) and observed by others (28,55,56). The restricted motion of the headgroups translates minimally to the carbons on the acyl chains near the glycerol backbone, causing a slight increase and broadening in the transition temperature. This is what we would expect in the model where headgroups in PS microdomains are locked in position by the coordination of Ca^{2+}, while the acyl chains experience only slight restrictions on their motion. We propose that Ca^{2+} induces a more ordered liquid crystal phase in which there is increased order in the PS headgroups, while the acyl chains remain disordered as in a liquid phase. We picture this as a microdomain of PS in which diffusion of PS molecules within the microdomain is likely, and the microdomain, as a whole unit, is free to diffuse laterally in the bilayer. This is characterized in MD simulations presented in Figure 4 and is consistent with the dynamics data, including the increase and broadening of the liquid-crystalline to solid-gel phase transition temperature.

The intermolecular cross-peaks observed in homonuclear and heteronuclear correlation experiments (Figures 5 and 6) directly confirm a spatial reorganization of the PS headgroups. The <6 Å distance between Cα carbons and 6.1 Å distance between the ^{31}P of PS2 and ^{15}N of PS1 are in good agreement with the two major conformational populations observed in the MD simulations. We propose that the two conformations of the PS headgroup are arranged in a twofold symmetry around a shared Ca^{2+} coordination center (Figure 7). This model is also consistent with binding data and previously reported MD simulations showing a 2:1 ratio of PS:Ca^{2+} (10, 30, 66), although the exact stoichiometry of the coordination center is yet to be determined.

In conclusion, we have demonstrated that Ca^{2+} interacts with PS in membrane bilayers to form more ordered PS microdomains. The interaction induces a symmetric organization of the PS in the lipid bilayer, which is free to diffuse laterally through the bilayer. By studying these microscopic and transient islands of a specific PS lipid, we will be able to better understand the membrane's contribution to processes such as cell signaling and blood coagulation (14,15). Specifically, we will be able to determine the conformations of the PS headgroups in Ca^{2+}-bound microdomains that may be encountered by PS-specific membrane binding proteins. Our current work is focused on completing the analysis of distance and angular restraints to use in calculations of an atomically resolved structure of the PS microdomains in membrane bilayers.

Acknowledgments

The authors would like to thank Drs. Stephen Sligar and Aleksandra Kijac for assistance with the Nanodisc system; Lindsay J. Sperling for help with NMR dynamics simulations; and Dr. Jennifer Rapp (NMR Facility, School of Chemical Sciences, University of Illinois at Urbana-Champaign) for assisting in acquisition of experiments; and Drs. Anna Nesbitt and Taras Pogorelov for careful reading of the manuscript. YZO and ET thank Geoff Christensen for preliminary data generation and analysis. All the simulations were performed using computer time on TeraGrid resources (grant MCA06N060).

Abbreviations

Cα	alpha carbon
Cβ	beta carbon
Cγ	gamma carbon

CP	cross-polarization
DARR	dipolar assisted rotational resonance
DMPS	1,2-dimyristoyl-phosphatidylserine
DOPS	1,2-dioleoyl-phosphatidylserine
DPC	dodecylphosphocholine
GLA	γ-carboxyglutamate-rich domain
MAS	magic-angle spinning
MD	molecular dynamics
MSP	membrane scaffold protein
PIP_2	phosphatidylinositol-4,5-bisphosphate
PKCα	protein kinase C isoform α
PLD	phospholipase D
POPC	1-palmitoyl-2-oleoyl-phosphatidylcholine
POPS	1-palmitoyl-2-oleoyl-phosphatidylserine
POPS*	POPS with uniformly ^{13}C, ^{15}N-labeled L-serine
PS	phosphatidylserine
REDOR	rotational-echo double resonance
SSNMR	solid-state nuclear magnetic resonance
TEDOR	transferred-echo double resonance
TPPM	two-pulse phase modulation
T_2	transverse relaxation

References

1. Gordesky SE, Marinetti GV. The asymetric arrangement of phospholipids in the human erythrocyte membrane. Biochem Biophys Res Commun. 1973; 50:1027–1031. [PubMed: 4690843]
2. Buckland AG, Wilton DC. Anionic phospholipids, interfacial binding and the regulation of cell functions. Biochim Biophys Acta. 2000; 1483:199–216. [PubMed: 10634937]
3. Leventis PA, Grinstein S. The distribution and function of phosphatidylserine in cellular membranes. Annu Rev Biophys. 2010; 39:407–427. [PubMed: 20192774]
4. McLaughlin S, Murray D. Plasma membrane phosphoinositide organization by protein electrostatics. Nature. 2005; 438:605–611. [PubMed: 16319880]
5. Yeung T, Gilbert GE, Shi J, Silvius J, Kapus A, Grinstein S. Membrane phosphatidylserine regulates surface charge and protein localization. Science. 2008; 319:210–213. [PubMed: 18187657]
6. Lemmon MA. Membrane recognition by phospholipid-binding domains. Nat Rev Mol Cell Biol. 2008; 9:99–111. [PubMed: 18216767]
7. Fadok VA, Voelker DR, Campbell PA, Cohen JJ, Bratton DL, Henson PM. Exposure of phosphatidylserine on the surface of apoptotic lymphocytes triggers specific recognition and removal by macrophages. J Immunol. 1992; 148:2207–2216. [PubMed: 1545126]
8. Zwaal RF, Comfurius P, Bevers EM. Surface exposure of phosphatidylserine in pathological cells. Cell Mol Life Sci. 2005; 62:971–988. [PubMed: 15761668]

9. Duzgunes N, Nir S, Wilschut J, Bentz J, Newton C, Portis A, Papahadjopoulos D. Calcium- and magnesium-induced fusion of mixed phosphatidylserine/phosphatidylcholine vesicles: effect of ion binding. J Membr Biol. 1981; 59:115–125. [PubMed: 7241577]
10. Feigenson GW. On the Nature of Calcium-Ion Binding between Phosphatidylserine Lamellae. Biochemistry-US. 1986; 25:5819–5825.
11. Leckband DE, Helm CA, Israelachvili J. Role of calcium in the adhesion and fusion of bilayers. Biochemistry-US. 1993; 32:1127–1140.
12. Ito T, Ohnishi SI. Ca2+-Induced Lateral Phase Separations in Phosphatic Acid-Phosphatidylcholine Membranes. Biochim Biophys Acta. 1974; 352:29–37. [PubMed: 4368475]
13. Berridge MJ, Irvine RF. Inositol trisphosphate, a novel second messenger in cellular signal transduction. Nature. 1984; 312:315–321. [PubMed: 6095092]
14. Maxfield FR. Plasma membrane microdomains. Curr Opin Cell Biol. 2002; 14:483–487. [PubMed: 12383800]
15. Laude AJ, Prior IA. Plasma membrane microdomains: organization, function and trafficking. Mol Membr Biol. 2004; 21:193–205. [PubMed: 15204627]
16. Menke M, Gerke V, Steinem C. Phosphatidylserine membrane domain clustering induced by annexin A2/S100A10 heterotetramer. Biochemistry-US. 2005; 44:15296–15303.
17. Schultz ZD, Pazos IM, McNeil-Watson FK, Lewis EN, Levin IW. Magnesium-induced lipid bilayer microdomain reorganizations: implications for membrane fusion. J Phys Chem B. 2009; 113:9932–9941. [PubMed: 19603842]
18. Gokhale NA, Abraham A, Digman MA, Gratton E, Cho W. Phosphoinositide specificity of and mechanism of lipid domain formation by annexin A2-p11 heterotetramer. J Biol Chem. 2005; 280:42831–42840. [PubMed: 16230353]
19. Eklund KK, Vuorinen J, Mikkola J, Virtanen JA, Kinnunen PKJ. Ca^{2+}-induced lateral phase separation in phosphatidic acid/phosphatidylcholine monolayers as revealed by fluorescence microscopy. 1988
20. Levental I, Christian DA, Wang YH, Madara JJ, Discher DE, Janmey PA. Calcium-dependent lateral organization in phosphatidylinositol 4,5-bisphosphate (PIP2)- and cholesterol-containing monolayers. Biochemistry-US. 2009; 48:8241–8248.
21. Roux M, Bloom M. Ca^{2+}, Mg^{2+}, Li^{+}, Na^{+}, and K^{+} distributions in the headgroup region of binary membranes of phosphatidylcholine and phosphatidylserine as seen by deuterium NMR. Biochemistry-US. 1990; 29:7077–7089.
22. Roux M, Bloom M. Calcium-binding by phosphatidylserine headgroups - Deuterium NMR study. Biophys J. 1991; 60:38–44. [PubMed: 1883944]
23. Sanson A, Monck MA, Neumann JM. 2D H-1-NMR conformational study of phosphatidylserine diluted in perdeuterated dodecylphosphocholine micelles - Evidence for a pH-Induced conformational transition. Biochemistry-US. 1995; 34:5938–5944.
24. Frazier AA, Roller CR, Havelka JJ, Hinderliter A, Cafiso DS. Membrane-bound orientation and position of the synaptotagmin I C2A domain by site-directed spin labeling. Biochemistry-US. 2003; 42:96–105.
25. Rufener E, Frazier AA, Wieser CM, Hinderliter A, Cafiso DS. Membrane-bound orientation and position of the synaptotagmin C2B domain determined by site-directed spin labeling. Biochemistry-US. 2005; 44:18–28.
26. Verdaguer N, Corbalan-Garcia S, Ochoa WF, Fita I, Gomez-Fernandez JC. Ca^{2+} bridges the C2 membrane-binding domain of protein kinase Cα directly to phosphatidylserine. EMBO J. 1999; 18:6329–6338. [PubMed: 10562545]
27. Ohkubo YZ, Tajkhorshid E. Distinct structural and adhesive roles of Ca^{2+} in membrane binding of blood coagulation factors. Structure. 2008; 16:72–81. [PubMed: 18184585]
28. Sinn CG, Antonietti M, Dimova R. Binding of calcium to phosphatidylcholine-phosphatidylserine membranes. Colloid Surface A. 2006; 282:410–419.
29. Pedersen UR, Leidy C, Westh P, Peters GH. The effect of calcium on the properties of charged phospholipid bilayers. Biochim Biophys Acta. 2006; 1758:573–582. [PubMed: 16730642]

30. Vernier PT, Ziegler MJ, Dimova R. Calcium Binding and Head Group Dipole Angle in Phosphatidylserine-Phosphatidylcholine Bilayers. Langmuir. 2009; 25:1020–1027. [PubMed: 19063658]

31. Bayburt TH, Sligar SG. Self-assembly of single integral membrane proteins into soluble nanoscale phospholipid bilayers. Prot Sci. 2003; 12:2476–2481.

32. Bayburt TH, Sligar SG. Single-molecule height measurements on microsomal cytochrome P450 in nanometer-scale phospholipid bilayer disks. Proc Natl Acad Sci U S A. 2002; 99:6725–6730. [PubMed: 11997441]

33. Bayburt TH, Grinkova YV, Sligar SG. Self-assembly of discoidal phospholipid bilayer nanoparticles with membrane scaffold proteins. Nano Lett. 2002; 2:853–856.

34. Bayburt TH, Carlson JW, Sligar SG. Single molecule height measurements on a membrane protein in nanometer-scale phospholipid bilayer disks. Langmuir. 2000; 16:5993–5997.

35. Morrissey JH, Pureza V, Davis-Harrison RL, Sligar SG, Ohkubo YZ, Tajkhorshid E. Blood clotting reactions on nanoscale phospholipid bilayers. Thromb Res. 2008; 122(Suppl 1):S23–26. [PubMed: 18691494]

36. Morrissey JH, Pureza V, Davis-Harrison RL, Sligar SG, Rienstra CM, Kijac AZ, Ohkubo YZ, Tajkhorshid E. Protein-membrane interactions: blood clotting on nanoscale bilayers. J Thromb Haemost. 2009; 7:169–172. [PubMed: 19630793]

37. Li Y, Kijac AZ, Sligar SG, Rienstra CM. Structural analysis of nanoscale self-assembled discoidal lipid bilayers by solid-state NMR spectroscopy. Biophys J. 2006; 91:3819–3828. [PubMed: 16905610]

38. Frericks HL, Zhou DH, Yap LL, Gennis RB, Rienstra CM. Magic-angle spinning solid-state NMR of a 144 kDa membrane protein complex: E-coli cytochrome bo_3 oxidase. J Biomol NMR. 2006; 36:55–71. [PubMed: 16964530]

39. Kijac AZ, Li Y, Sligar SG, Rienstra CM. Magic-Angle Spinning Solid-State NMR Spectroscopy of Nanodisc-Embedded Human CYP3A4. Biochemistry-US. 2007; 46:13696–13703.

40. Iwasaki Y, Mizumoto Y, Okada T, Yamamoto T, Tsutsumi K, Yamane T. An aqueous suspension system for phospholipase D-mediated synthesis of PS without toxic organic solvent. J Am Oil Chem Soc. 2003; 80:653–657.

41. Comfurius P, Zwaal RFA. Enzymatic-Synthesis of Phosphatidylserine and Purification by Cm-Cellulose Column Chromatography. Biochim Biophys Acta. 1977; 488:36–42. [PubMed: 560868]

42. Van Geet AL. Calibration of the methanol and glycol nuclear magnetic resonance thermometers with a static thermistor probe. Anal Chem. 1968; 42:2227.

43. Hediger S, Meier BH, Kurur ND, Bodenhausen G, Ernst RR. NMR cross-polarization by adiabatic passage through the Hartmann-Hahn condition (APHH). Chem Phys Lett. 1994; 223:283–288.

44. Bennett AE, Rienstra CM, Auger M, Lakshmi KV, Griffin RG. Heteronuclear decoupling in rotating solids. J Chem Phys. 1995; 103:6951–6958.

45. Delaglio F, Grzesiek S, Vuister GW, Zhu G, Pfeifer J, Bax A. Nmrpipe: a Multidimensional Spectral Processing System Based On Unix Pipes. J Biomol NMR. 1995; 6:277–293. [PubMed: 8520220]

46. Morcombe CR, Zilm KW. Chemical shift referencing in MAS solid state NMR. J Magn Reson. 2003; 162:479–486. [PubMed: 12810033]

47. Goddard, TD.; Kneller, DG. Sparky 3. 3.106. University of California; San Francisco:

48. Phillips JC, Braun R, Wang W, Gumbart J, Tajkhorshid E, Villa E, Chipot C, Skeel RD, Kale L, Schulten K. Scalable molecular dynamics with NAMD. J Comput Chem. 2005; 26:1781–1802. [PubMed: 16222654]

49. MacKerell AD, Bashford D, Bellott, Dunbrack RL, Evanseck JD, Field MJ, Fischer S, Gao J, Guo H, Ha S, Joseph-McCarthy D, Kuchnir L, Kuczera K, Lau FTK, Mattos C, Michnick S, Ngo T, Nguyen DT, Prodhom B, Reiher WE, Roux B, Schlenkrich M, Smith JC, Stote R, Straub J, Watanabe M, Wiorkiewicz-Kuczera J, Yin D, Karplus M. All-atom empirical potential for molecular modeling and dynamics studies of proteins. J Phys Chem B. 1998; 102:3586–3616.

50. Darden TA, York DM, Pedersen L. Particle mesh Ewald: An N.log(N) method for Ewald sums in large systems. J Chem Phys. 1993; 98:10089–10092.

51. Petrache HI, Tristram-Nagle S, Gawrisch K, Harries D, Parsegian VA, Nagle JF. Structure and fluctuations of charged phosphatidylserine bilayers in the absence of salt. Biophys J. 2004; 86:1574–1586. [PubMed: 14990484]
52. Wang, Y.; Ohkubo, YZ.; Tajkhorshid, E. Gas conduction of lipid bilayers and membrane channels. In: Feller, S., editor. Current Topics in Membranes: Computational Modeling of Membrane Bilayers. Elsevier; 2008. p. 343-367.
53. Husted C, Montez B, Le C, Moscarello MA, Oldfield E. C-13 Magic-angle sample-spinning nuclear-magnetic-resonance studies of human myelin, and model membrane systems. Magnet Reson Med. 1993; 29:168–178.
54. Denisov IG, McLean MA, Shaw AW, Grinkova YV, Sligar SG. Thermotropic phase transition in soluble nanoscale lipid bilayers. J Phys Chem B. 2005; 109:15580–15588. [PubMed: 16852976]
55. Jacobson K, Papahadjopoulos D. Phase-transitions and phase separations in phospholipid membranes induced by changes in temperature, pH, and concentration of bivalent-cations. Biochemistry-US. 1975; 14:152–161.
56. Silvius JR, Gagne J. Calcium-induced fusion and lateral phase separations in phosphatidylcholine-phosphatidylserine vesicles - correlation by calorimetric and fusion measurements. Biochemistry-US. 1984; 23:3241–3247.
57. Zhao X, Eden M, Levitt MH. Recoupling of heteronuclear dipolar interactions in solid-state NMR using symmetry-based pulse sequences. Chem Phys Lett. 2001; 342:353–361.
58. Takegoshi K, Nakamura S, Terao T. C-13-H-1 dipolar-assisted rotational resonance in magic-angle spinning NMR. Chem Phys Lett. 2001; 344:631–637.
59. Morcombe CR, Gaponenko V, Byrd RA, Zilm KW. Diluting abundant spins by isotope edited radio frequency field assisted diffusion. J Am Chem Soc. 2004; 126:7196–7197. [PubMed: 15186155]
60. Hing A, Vega S, Schaefer J. Transferred-echo double-resonance NMR. J Magn Reson. 1992; 96:205–209.
61. Lange A, Luca S, Baldus M. Structural constraints from proton-mediated rare-spin correlation spectroscopy in rotating solids. J Am Chem Soc. 2002; 124:9704–9705. [PubMed: 12175218]
62. Lange A, Seidel K, Verdier L, Luca S, Baldus M. Analysis of proton-proton transfer dynamics in rotating solids and their use for 3D structure determination. J Am Chem Soc. 2003; 125:12640–12648. [PubMed: 14531708]
63. Jaroniec CP, Filip C, Griffin RG. 3D TEDOR NMR experiments for the simultaneous measurement of multiple carbon-nitrogen distances in uniformly C-13, N-15-labeled solids. J Am Chem Soc. 2002; 124:10728–10742. [PubMed: 12207528]
64. Hauser H, Pascher I, Sundell S. Preferred Conformation and Dynamics of the Glycerol Backbone in Phospholipids - an NMR and X-ray single-crystal analysis. Biochemistry-US. 1988; 27:9166–9174.
65. Browning JL, Seelig J. Bilayers of phosphatidylserine - deuterium and phosphorus nuclear magnetic-resonance study. Biochemistry-US. 1980; 19:1262–1270.
66. Mattai J, Hauser H, Demel RA, Shipley GG. Interactions of metal-ions with phosphatidylserine bilayer-membranes - effect of hydrocarbon chain unsaturation. Biochemistry-US. 1989; 28:2322–2330.

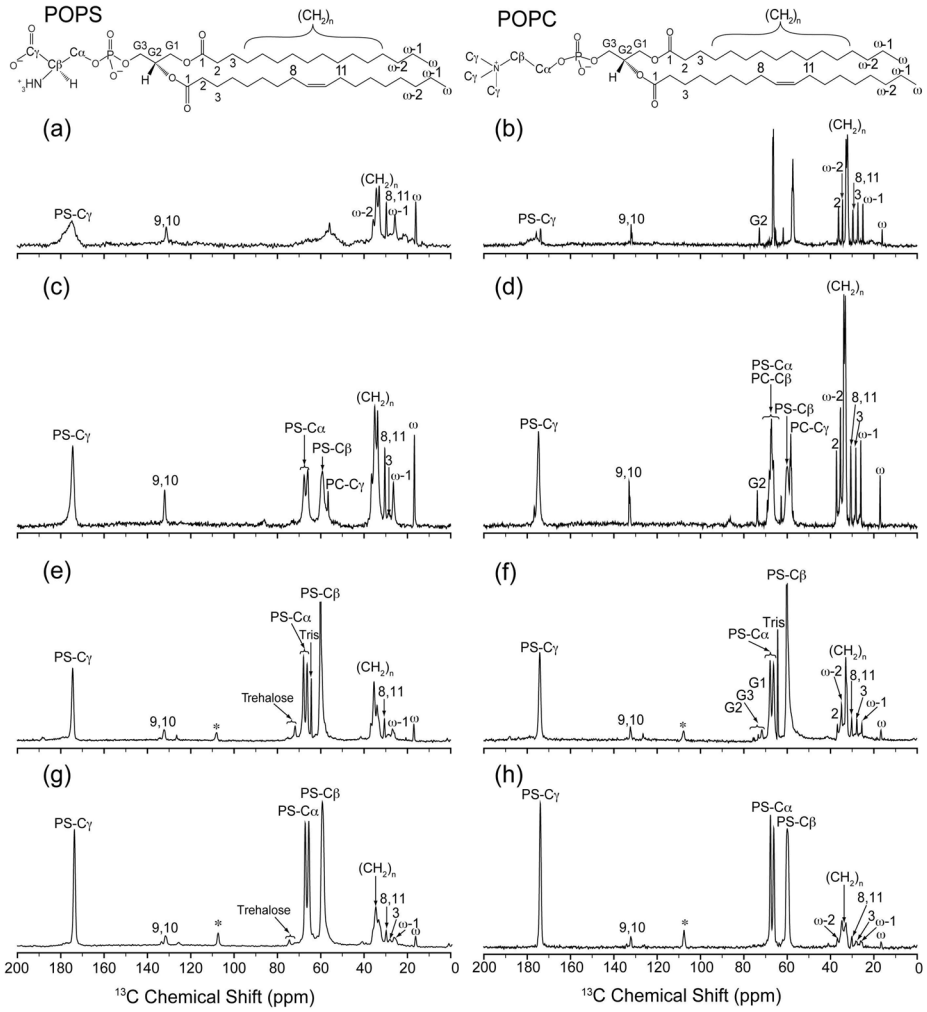

Figure 1.

Effect of Ca^{2+} and temperature on cross-polarized ^{13}C one-dimensional spectra of phospholipid bilayers. Spectra of 30% POPS*, 70% POPC liposomes were acquired without Ca^{2+} at (a) −20 °C or (b) 10 °C; or with 2.5 mM Ca^{2+} at (c) −20 °C or (d) 10 °C. Spectra of Nanodiscs were all acquired with 2 mM Ca^{2+}, using 30% POPS*, 70% POPC Nanodiscs at (e) −20 °C or (f) 10 °C; or 70% POPS*, 30% POPC Nanodiscs at (g) −20 °C or (h) 10 °C, Spectra (a)–(d) were acquired with an MAS rate of 11.111 kHz on a 500 MHz (^1H frequency) spectrometer. Spectra (e)–(h) were acquired with an MAS rate of 10.000 kHz on a 600 MHz (^1H frequency) spectrometer; asterisks indicate a carrier frequency artifact at ~108 ppm. All spectra were zero filled to twice the original data size and line broadened 0.2 ppm.

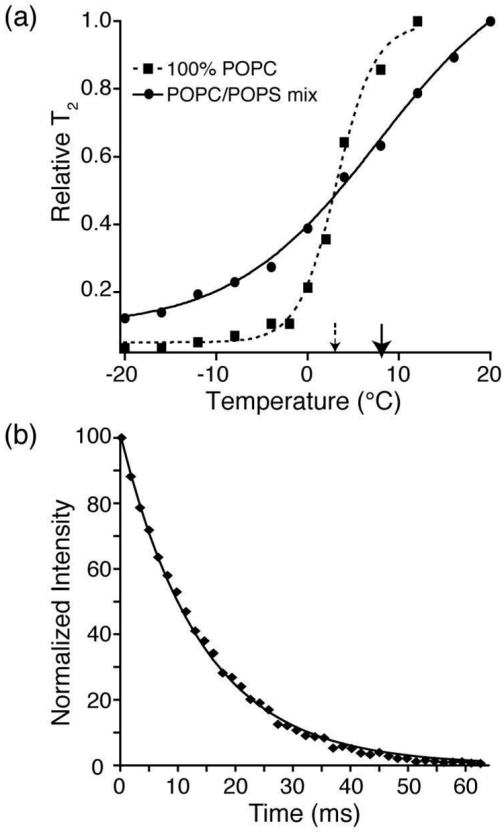

Figure 2.

(a) Normalized ^{1}H T_2 values of the bulk fatty acyl CH_2 peaks of nanobilayers, as a function of temperature. Nanodiscs were composed of either 100% POPC (squares, dashed lines) or 30% POPS*, 70% POPC (circles, solid lines) with 2 mM Ca^{2+}. Transition temperatures were determined using acyl chain signals, with ^{1}H T_2 values used to fit the inflection point of the curve as a function of temperature. The solid arrow denotes the phase transition for 30% POPS*, 70% POPC Nanodiscs (~8 °C), while the dashed arrow denotes the phase transition for 100% POPC Nanodiscs (~3 °C). (b) ^{1}H Hahn echo was used to investigate the T_2 of the methylene protons (8 and 11; Figure 1) neighboring the olefinic bond at 25 °C. Plotted is the intensity of the methylene proton peak as a function of the echo time. A single exponential decay curve was fitted (using Spinsight 3.0); a bi-exponential fit did not yield statistically significant improvement (F test). The T_2 was determined to be 14 ms.

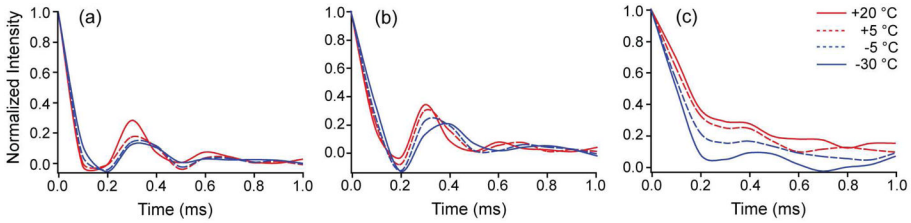

Figure 3.

Dipolar dephasing trajectories of phospholipid headgroups and acyl chains in 30% POPS*, 70% POPC Nanodiscs with 2 mM Ca^{2+}. ^{1}H-^{13}C dipolar trajectories (plotted as normalized intensities) are presented at the indicated temperatures for (a) the Cα (CH_2) of the serine headgroup, (b) the Cβ (CH) of the serine headgroup, and (c) the bulk CH_2 (same resonance used in Figure 2b) of fatty acyl chains. The ^{1}H-^{13}C dipolar interaction was recoupled using $R18_1^7$ in a constant time manner. The PS headgroup maintains an order parameter near the rigid lattice limit (S = ~0.9), while the acyl chain motion is substantially activated (S = ~0.6 to 0.9) over the range from −30 °C to +20 °C.

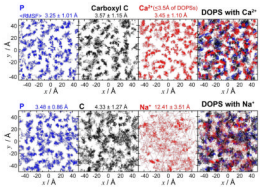

Figure 4.

Structure and dynamics of lipid molecules. Top view of one of the leaflets of the DOPS membranes simulated with either Ca^{2+} (top panel) or Na^{+} (bottom panel) as counterion. The leftmost panels show the trajectories of phosphorus atoms of the phosphate groups in blue lines, using positions taken every 0.2 ns from the last 90 ns of the 100 ns simulations. Using the same snapshots, in the second panels the trajectories of the carboxyl carbons are shown in black, and in the third panels the trajectories of the counterions within 3.5 Å of DOPS lipids are depicted in red. The right-most panels show the overlap of the three sets of trajectories. The average root-mean-square fluctuations (RMSFs) of the atoms used in each panel are also shown. Due to the large number of frames included in the analysis and in order to avoid overcrowding that would mask the differences between the two systems, in each case, only half of the lipids (72 out of 144) were randomly selected for the analysis of phosphorus and carboxyl carbon atoms.

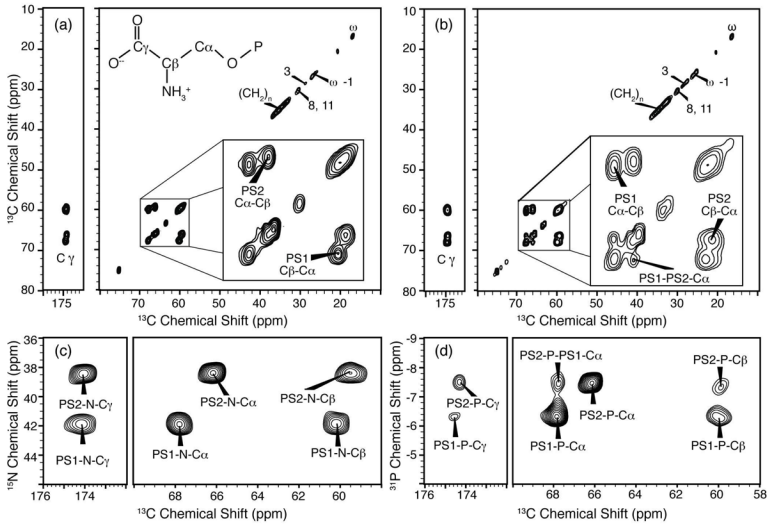

Figure 5.

Ca^{2+} induces two conformations of PS headgroups as evidenced by two-dimensional SSNMR. Spectra were acquired of 70% POPS*, 30% POPC Nanodiscs with 2 mM Ca^{2+} using an MAS rate of 10 kHz on a 600 MHz (^{1}H frequency) spectrometer: ^{13}C-^{13}C two-dimensional DARR spectra with (a) 25 ms DARR mixing acquired at −30 °C and (b) with 200 ms DARR mixing acquired at 5 °C. Insets in panels a and b are expansions of Cα-Cβ regions. The phosphorus and nitrogen chemical shifts of the two Ca^{2+}-induced conformers are also well resolved as shown in expansions of the serine Cα-Cβ and Cγ regions of (c) ^{15}N-^{13}C TEDOR spectrum with 6.4 ms REDOR mixing acquired at −20 °C and (d) ^{31}P-^{13}C TEDOR spectrum with 2.4 ms of REDOR mixing acquired at −20 °C. All spectra were zero filled to twice the original data size. The ^{13}C-^{13}C two-dimensional spectra were line broadened 0.2 ppm in each dimension. The ^{31}P-^{13}C and ^{15}N-^{13}C spectra were line broadened 0.4 ppm in the carbon dimension and 0.25 ppm in the ^{31}P and/or ^{15}N dimensions.

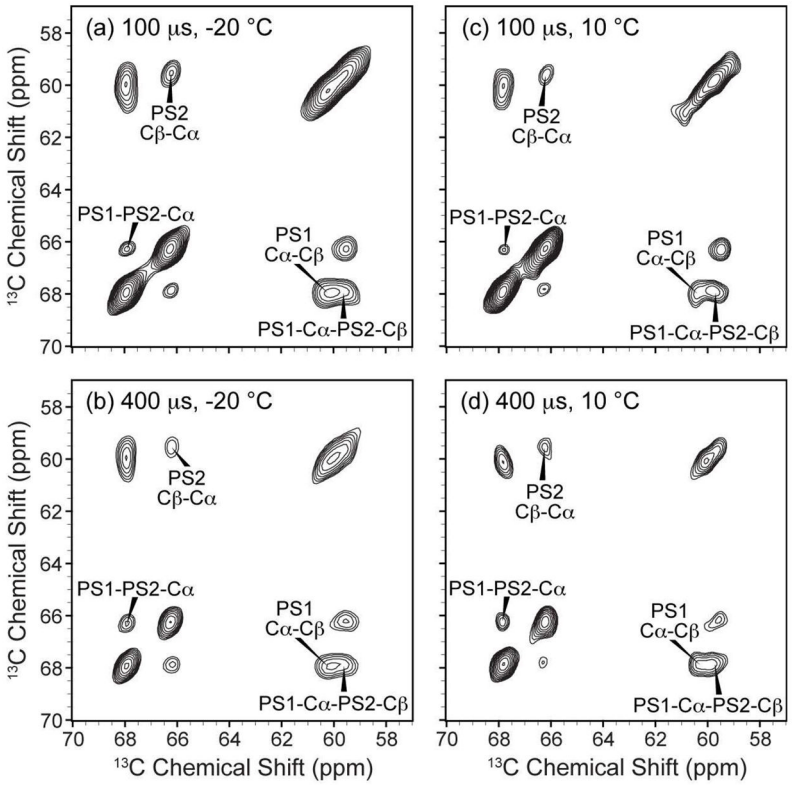

Figure 6.

Close intermolecular ^{13}C-^{13}C spacing between the two configurations of the PS headgroup, demonstrated by intermolecular cross-peaks in CHHC two-dimensional correlation spectra of 70% POPS* 30% POPC Nanodisc prepared with 2 mM Ca^{2+}. Gel phase spectra (left) were acquired at −20 °C and liquid crystal phase spectra (right) were acquired at 10 °C with (a, c) 100 μs and (b, d) 400 μs of ^{1}H-^{1}H mixing. All spectra were acquired with an MAS rate of 10 kHz on a 600 MHz (^{1}H frequency) spectrometer, and processed with 0.3 ppm of line broadening in each dimension.

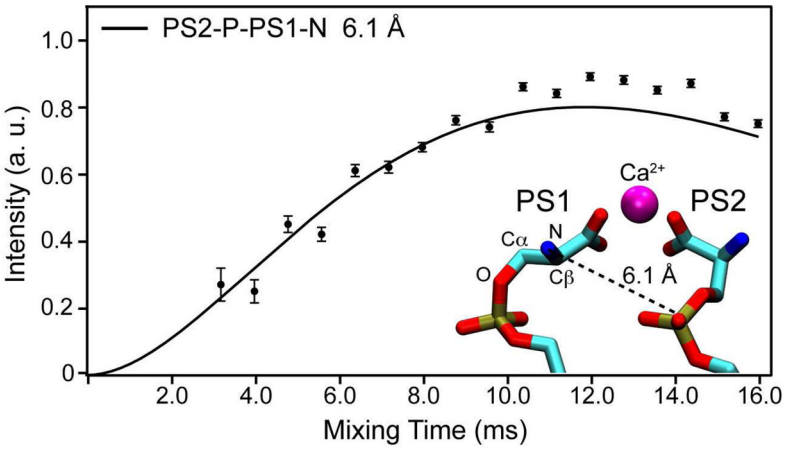

Figure 7.

Three-dimensional ZF TEDOR trajectories of the cross-peak observed for the ^{31}P of the PS2 and the ^{15}N of the PS1 headgroup spin systems with a T_2 of 7.0 ms. To derive distance values, experimental buildup curves were fitted using a nonlinear least-squares optimization of the analytical expression described by equations 10 & 11 in Jaroniec et al. (63). Also shown as an insert is a snapshot taken from the MD simulations depicting an example of a PS1 and a PS2 headgroup interacting with the same Ca^{2+} ion. The O-Cα-Cβ-N dihedral angle and the Cγ-P distance are −71.2° and 4.82 Å in PS1 (left), and 52.4° and 4.17 Å in PS2 (right). The distance between PS1-N and PS2-P in this snapshot is 6.05 Å.

Table 1

Carbon, nitrogen and phosphorus chemical shift values for PS headgroups bound to Ca^{2+} in mixed POPS:POPC bilayers.[a]

	Chemical Shift Values (ppm)				
	Cα	**Cβ**	**Cγ**	**N**	**P**
PS1	67.9	60.2	174.4	41.8	−6.3
PS2	66.3	59.6	174.2	38.4	−7.4

[a]The chemical shift values were assigned using the spectra in Figure 5.